Chemistry and Physics of Lipids 157 (2009) 40–50

Contents lists available at ScienceDirect

Chemistry and Physics of Lipids

journal homepage: www.elsevier.com/locate/chemphyslip

The solid–liquid phase diagrams of binary mixtures of consecutive, even saturated fatty acids: differing by four carbon atoms

Mariana C. Costa[a,b], Mariana Sardo[b], Marlus P. Rolemberg[c], Paulo Ribeiro-Claro[b], Antonio J.A. Meirelles[d], João A.P. Coutinho[b], M.A. Krähenbühl[a,*]

[a] LPT, Department of Chemical Process, School of Chemical Engineering, State University of Campinas, UNICAMP, P.O. Box 6066, 13083-970 Campinas, SP, Brazil
[b] CICECO, Departamento de Química da Universidade de Aveiro, 3810-193 Aveiro, Portugal
[c] DETQI, Department of Chemical Technology, Federal University of Maranhão (UFMA), São Luís, Maranhão, Brazil
[d] EXTRAE, Department of Food Engineering, School of Food Engineering, State University of Campinas, UNICAMP, P.O. Box 6121, 13083-862 Campinas, SP, Brazil

ARTICLE INFO

Article history:
Received 15 April 2008
Accepted 25 September 2008
Available online 17 October 2008

Keywords:
Solid–liquid equilibrium
Saturated fatty acids
Phase diagram
DSC
XRD
FT-Raman

ABSTRACT

The complete solid–liquid phase diagrams for four binary mixtures of saturated fatty acids are presented, for the first time, in this work. These mixtures are formed by caprylic acid ($C_{8:0}$) + lauric acid ($C_{12:0}$), capric acid ($C_{10:0}$) + myristic acid ($C_{14:0}$), lauric acid ($C_{12:0}$) + palmitic acid ($C_{16:0}$) and myristic acid ($C_{14:0}$) + stearic acid ($C_{18:0}$). The phase diagrams were obtained by differential scanning calorimetry (DSC) and X-ray diffraction (XRD). FT-Raman spectrometry and polarized light microscopy were used to complement the characterization for a complete understanding of the phase diagram. All of the phase diagrams here reported show the same global behavior that is far more complex than previously accepted. They present not only peritectic and eutectic reactions, but also metatectic reactions, due to solid–solid phase transitions common in fatty acids, and regions of solid solution not previously reported. This work contributes to the elucidation of the phase behavior of these important biochemical molecules with implications in various industrial applications.

1. Introduction

This is the second part of a series of works (Costa et al., accepted for publication) concerning the solid–liquid equilibrium (SLE) of fatty acids binary mixtures. In this work the complete phase diagrams of binary mixtures of saturated fatty acids with a difference of four carbon atoms between the chains are established using DSC measurements complemented by FT-Raman spectroscopy, X-ray diffraction (XRD) studies and polarized light microscopy. Fatty acids have been the focus of intense researches since the early 1900s because they are the major components of oils and fats (Karleskind, 1996). Lately, an accrued interest on these compounds results from their application for the production of coatings, plastics, cleaning products (Johnson and Fritz, 1989), phase change materials for energy storage (Zhang et al., 2001; Shilei et al., 2006), and biodiesel (Falk and Meyer-Pittroff, 2004; Meher et al., 2006).

The utilization of fatty acids in the chemical, food and pharmaceutical industries (Carvalho et al., 2006; Kogan and Garti, 2006), requires a good knowledge of their properties and phase behavior. In particular in the food industry, the phase behavior and crystalline habit of the fatty acid mixtures influences the characteristics of consumer products such as confectionary fats.

The polymorphism of triglycerides and fatty acids is well known since long, but the study of the crystal forms of pure fatty acids dates only from the 1950s and still is a challenging task (Vand et al., 1951; Holland and Nielsen, 1963; Lomer, 1963; Goto and Asada, 1978a, 1978b; Kaneko et al., 1990; Moreno et al., 2007). Researchers worldwide have been addressing the study of the thermal properties and behavior of solid fats (Chapman, 1962; Timms, 1984; Garti and Sato, 1989; Sato et al., 1999; Sato, 2001), and the phase diagram of fats (Bailey, 1950; Timms, 1984; Small, 1986; Sato et al., 1999; Sato, 2001) and fatty acids (Inoue et al., 2004a,b,c; Costa et al., 2007b).

Concerning the phase diagrams of fatty acid binary mixtures Bailey (1950) and Small (1986) reported the existence of two invariant points, eutectic and peritectic. The phase diagrams of binary mixtures of fatty acids was suggested to be a simple eutectic for systems with chains length differences equal or larger than six carbon atoms, while for the others the presence of an intermediate compound unstable at the melting point originated a peritectic point

* Corresponding author. Tel.: +55 19 3521 3964; fax: +55 19 3521 3965.
E-mail addresses: mccosta@feq.unicamp.br (M.C. Costa), msardo@ua.pt (M. Sardo), marlus@ufma.br (M.P. Rolemberg), prc@ua.pt (P. Ribeiro-Claro), tomze@fea.unicamp.br (A.J.A. Meirelles), jcoutinho@ua.pt (J.A.P. Coutinho), mak@feq.unicamp.br (M.A. Krähenbühl).

0009-3084/$ – see front matter © 2008 Elsevier Ireland Ltd. All rights reserved.
doi:10.1016/j.chemphyslip.2008.09.006

(Small, 1986; Iwahashi et al., 2005). In our recent works (Costa et al., 2007a,b) the presence of these invariant points was also observed. However, while revisiting the phase diagrams of binary mixtures of fatty acids using DSC (Costa et al., 2007b) a number of indications that the phase diagrams for these mixtures were far more complex than previously admitted were collected, prompting these studies where other techniques, such as FT-Raman spectroscopy, XRD studies and polarized light microscopy, were used to elucidate the complete phase diagram of binary mixtures of fatty acids below the saturation line. A complete phase diagram will be here proposed and it will be shown that the phase diagram of these mixtures is far more complex than previously admitted.

2. Experimental

2.1. Materials

Standards used for calibration of the DSC were indium (99.999%) certified by TA instruments (United States); cyclohexane (min 99.99%) and naphthalene (min 99%), both from Merck (Germany). The fatty acids used to prepare the samples were high purity and were obtained from the following suppliers: caprylic acid (min 99%), capric acid (min 99%), lauric acid (99–100%), myristic acid (99–100%), palmitic acid (min 99%) and stearic acid (min 99%) was used on the diffractometer and on the spectrometer – Sigma–Aldrich (United States); stearic acid (min 97%) – Merck (Germany) was used on the DSC. Commercial nitrogen (used for preparing binary samples) and high purity nitrogen (used in the calorimeter) were supplied by Air Liquide (Brazil).

2.2. Preparation of fatty acid binary mixtures

The samples used in this work were prepared on an analytical balance (Adam AAA/L) with a ±0.2 mg accuracy. The weighed compounds were placed in a glass tube, and heated and stirred under a nitrogen atmosphere until 10 K above the higher melting point of the components. The mixtures were then allowed to cool to room temperature and kept in a freezer at 273 K until analysis.

For the FT-Raman spectra recorded before melting (BM) the samples were just weighed and mixed in the solid state by crushing the crystals in a mortar. The melting of these samples was carried in the spectrophotometer, inside the capillary tube used for the analysis, after recording the BM spectra, at a temperature circa 10 K above the melting point of the heaviest compound. The samples were then cooled inside the spectrophotometer to the desired temperature to acquire the spectra after mixing the compounds in the liquid phase and the formation of new mixed crystals.

2.3. Differential scanning calorimetry (DSC)

The solid–liquid equilibrium of pure fatty acids and their mixtures were characterized by DSC, using a MDSC 2920, TA Instruments calorimeter. The experimental procedure was described in detail in a previous work (Costa et al., 2007b). The average absolute deviations between measurements were estimated to range from 0.03 to 0.06 K for all the standards and from 0.03 to 0.2 K for the mixtures, the uncertainty of the phase equilibrium data was estimated to be inferior to 0.2 K.

2.4. X-ray diffraction

The fatty acids diffractograms were obtained in a Philips X'Pert equipment which operates in the reflection mode with Cu Kα (λ = 1.5406 Å). The cooled chamber is an Anton Paar TTK450, the temperature controller is a TCU100 and the chamber was cooled using liquid nitrogen. Diffraction data were collected in a 2θ range from 4° to 50° in steps of 0.02 and a time per step of 2 s with incident and diffracted beam with anti-scatter slits of 1°, receiving slit of 0.1 mm and curved graphite diffracted beam monochromator.

2.5. Polarized light microscopy

A Leica (DM LM) light microscope was used to acquire the images. The images at ambient temperature were obtained using a polarized lens and transmitted light. The samples were prepared by melting the sample between two coverslips.

The images at controlled temperatures were obtained using a hot stage, Mettler FP82H, connected to the central processor unit of DSC Mettler Toledo FP 90.

2.6. FT-Raman spectroscopy

The spectra were recorded on a RFS-100 Bruker FT-Spectrometer, equipped with a Nd:YAG laser with excitation wavelength of 1064 nm, with laser power set to 400 mW. Each spectrum corresponds to a measurement of 400 scans and 2 cm^{-1} resolution.

In some experiments, it has been reported that the sample temperature can increase significantly due to laser exposure, which may subsequently lead to polymorphic transformations. Aiming at evaluating the effect of sample heating during measurements, a sample of each fatty acid was exposed continuously to 400 mW laser power for 4 h, during which several records of 5 min each were collected. The comparison of spectra shows that no change due to laser irradiation occurs in this time interval. Using the conditions previously described, all the FT-Raman spectra were collected in 45 min or less.

Samples were sealed in Kimax glass capillary tubes (0.8 mm i.d.). Temperature variation studies over the 273–353 K range were carried out with a commercial Harney–Miller-type assembly, and the temperature was monitored by the resistivity of a calibrated thermocouple. Under these circumstances, the error in temperature is estimated to be less than 0.5 K, with fluctuations during each recording below 1 K.

3. Results and discussion

3.1. Thermal analysis

The solid–liquid phase diagrams of four binary mixtures of even saturated fatty acids (caprylic acid (1) + lauric acid (3); capric acid (2) + myristic acid (4); lauric acid (3) + palmitic acid (5) and myristic acid (4) + stearic acid (6)) were investigated in this work. The results here obtained allowed to propose a global phase diagrams for these systems sketched in 1.

The *liquidus* lines of three of these systems were previously reported in the literature. Two of them, capric acid + myristic acid and lauric acid + palmitic acid systems were measured by us in a previous work using DSC (Costa et al., 2007b). For the other system, myristic acid + stearic acid, was measured by Heintz (Bailey, 1950) and the methodology used is not known. For this system only six experimental points were available. The other system, caprylic acid + myristic acid, had never previously been reported on the literature.

The thermograms of saturated fatty acids binary mixtures differing by four carbon atoms are as complex as the thermograms of mixtures differing by two carbon atoms studied in another part of the work (Costa et al., accepted for publication). The main difference between them is that the thermograms of the systems differing by four carbon atoms present one solid–solid transition below the

Table 1
Solid–liquid equilibrium data for caprylic acid (1) + lauric acid (2) system.

x_1	$T_{melting}$ (K)	$T_{peritectic}$ (K)	$T_{metatectic}$ (K)	$T_{eutectic}$ (K)	T_{trans1} (K)	T_{trans2} (K)	$T_{trans.pure}$ (K)
0.0000	318.07						317.56
0.1002	316.53	285.54	288.13		279.84	314.82	
0.2000	311.78	286.10	289.37		280.03		
0.3000	309.51	286.51	289.81		280.10		
0.3994	305.31	286.38	289.56		280.30	304.62	
0.5001	300.76	286.47	290.17		280.05		
0.5999	296.40	287.32	290.14		280.00		
0.7000	286.45			281.63	279.43		
0.7500	284.54			281.37	279.31		
0.7992	283.19			281.38	279.31		
0.8501	280.85				278.92		
0.9001	285.64			282.08	279.68		
1.0000	289.63						287.62

Table 2
Solid–liquid equilibrium data for capric acid (2) + myristic acid (4) system.

x_2	$T_{melting}$ (K)	$T_{peritectic}$ (K)	$T_{metatectic}$ (K)	$T_{eutectic}$ (K)	T_{trans1} (K)	T_{trans2} (K)	T_{trans2} (K)	$T_{trans.pure}$ (K)
0.0000	328.88							328.18
0.0986	325.01	300.1	303.38		295.03			
0.1968	322.49	300.6	304.46		295.85			
0.2997	319.72	301.00	304.69		296.01			
0.3985	316.49	301.2	305.10		295.35			
0.4979	313.53	301.32	305.49		295.36	308.52	311.15	
0.5986	302.08			297.11	295.37			
0.6490	301.50			297.25	295.60			
0.6996	300.39			297.39	295.85			
0.7992	296.78							
0.8475	296.85							
0.9013	300.69			297.11	295	299.46		
0.9505	302.31			296.57		299.72		
1.0000	304.42							

Table 3
Solid–liquid equilibrium data for lauric acid (3) + palmitic acid (5) system.

x_3	$T_{melting}$ (K)	$T_{peritectic}$ (K)	$T_{metatectic}$ (K)	$T_{eutectic}$ (K)	T_{trans1} (K)	$T_{trans.pure}$ (K)
0.0000	335.44					
0.1001	333.95	312.39	315.61		308.30	
0.2000	331.76	313.23	316.77		308.82	
0.3000	329.19	313.66	316.92		308.93	
0.4000	326.06	314.17	317.66		309.04	
0.5000	321.88	314.21	317.84		309.22	
0.5999	314.39			310.33		
0.6998	313.89			310.35		
0.7998	310.44					
0.8481	310.64					
0.8968	313.50			310.99		
1.0000	318.07					317.56

Table 4
Solid–liquid equilibrium data for myristic acid (4) + stearic acid (6) system.

x_4	$T_{melting}$ (K)	$T_{peritectic}$ (K)	$T_{metatectic}$ (K)	$T_{eutectic}$ (K)	T_{trans1} (K)	T_{trans2} (K)	$T_{trans.pure}$ (K)
0.0000	343.98						343.31
0.1001	341.19	322.21	325.76			317.62	
0.2000	339.27	323.28	326.69			319.23	
0.3001	336.96	323.75	327.00			319.37	
0.4001	334.14	324.15	327.57		331.13	319.56	
0.4999	332.09	324.19	327.47		329.75	319.76	
0.6002	326.70	324.53		320.87			
0.6273	324.08			320.84			
0.7003	323.10			320.80			
0.7894	320.68						
0.8000	321.38						
0.8997	324.49			321.13	321.98		
1.0000	328.88						328.18

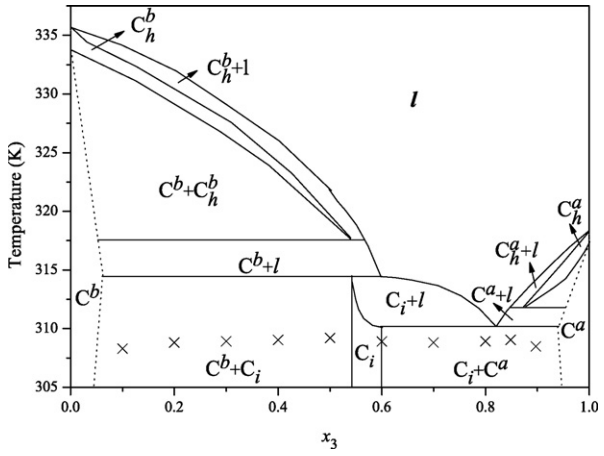

Fig. 1. Global phase diagram for the fatty acids systems studied in this work. *C* solid solution formed on the extremes of the phase diagram rich in one of the components of the mixture; C_i solid solution formed by the mixture of the components; C_h solid phase formed after the metatectic reaction; *l* liquid phase; × transition on the solid phase. The superscript *a* and *b* represents the components of the mixture.

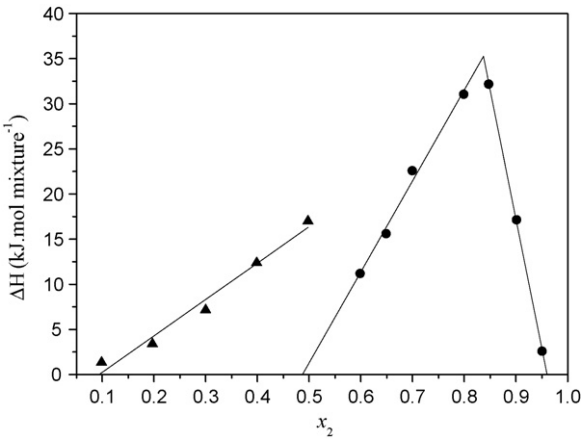

Fig. 3. Tamman plot for capric acid (2) + myristic acid (4) system. (▲) Enthalpy of the peritectic reaction; (●) enthalpy of the eutectic reaction; (—) fitting to the experimental results obtained.

eutectic temperature. This transition seems to occur in the entire concentration range but is particularly visible in the regions rich in the heavier compound. In the thermograms of the caprylic acid (1) + lauric acid (3) shown in Fig. 2 all transitions occurring before the complete melting of the sample are shown. For compositions of $x_1 \cong 0.20$ and $x_1 \cong 0.40$ is visible the presence of one peak before the peak of the peritectic point, which is indicated by an arrow. With the increase of the concentration in caprylic acid ($x_1 > 0.70$) the first peak of the thermogram, overlapped with the eutectic, results from the solid–solid transition occurring just before the eutectic point. The thermograms of the other systems studied in this work have an identical behavior, confirming the complexity of the phase diagrams of these systems, not coherent with the diagram of type 2-Ib2 previously proposed for them (Bailey, 1950; Small, 1986; Costa et al., 2007b).

The temperatures of all the endothermic peaks detected on the thermograms, usually associated with phase transitions, are reported in Tables 1–4 for each of the binary mixtures studied. In all cases they are coherent with the global phase diagram proposed although in some cases it was not possible to individualize all the phase transitions. The concentration ranges of the monophasic and biphasic regions are quite similar for all the binary mixtures with just temperatures translations among the different systems studied.

Thermograms for the systems studied in this work are similar to those previously presented for systems with a difference of two carbon atoms between the carbon chains (Costa et al., accepted for publication). The *liquidus* line of these systems presents two inflexion points, the peritectic point that appears at $x_1 \cong 0.60$ and the eutectic point at $x_1 \cong 0.80$. The presence of these two invariants on the liquidus line lead to the common interpretation that these diagrams would be of type 2-Ib2 according to the classification of Nývlt (1977). In the following discussion it will be shown

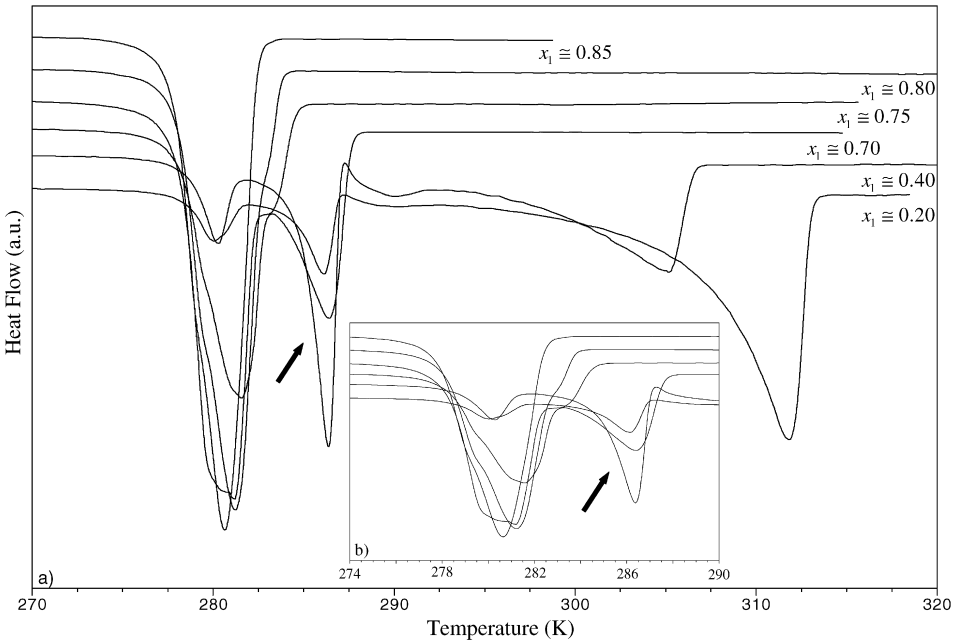

Fig. 2. (a) Thermograms for the system caprylic acid (1) + lauric acid (2); (b) inset of the thermograms around the peritectic and eutectic transition.

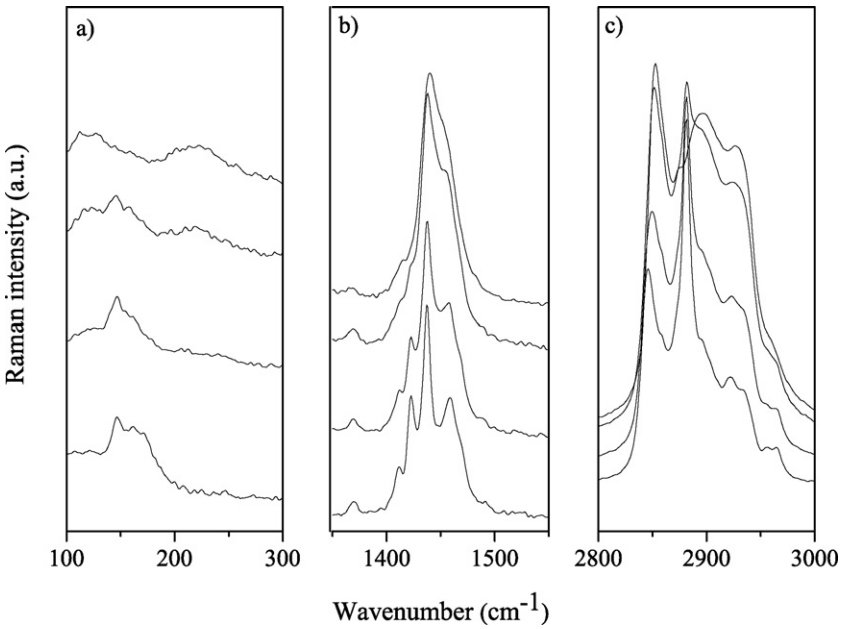

Fig. 4. Temperature dependence of the FT-Raman spectra for myristic acid (4) + stearic acid (6) system at $x_4 \cong 0.25$: (a) range 100–300 cm^{-1}; (b) range 1350–1550 cm^{-1}; (c) range 2800–3000 cm^{-1}. From bottom to top: 318.4, 322.15, 328.15 and 343.15 K.

that the results obtained by the experimental techniques used in this work are not compatible with this simplistic interpretation of the phase diagram (Bailey, 1950; Small, 1986; Costa et al., 2007b) and it will be shown how they support the peculiar features of the global phase diagram proposed in Fig. 1. Besides the eutectic and a peritectic invariants observed at concentrations of ≅0.8 and ≅0.6 molar fractions, respectively, for all the systems here reported it is still possible to identify:

- Two metatectic invariants, observed at concentrations not fully determined in this work but for which the temperatures are known for most systems studied. One of these is observed at a composition below the peritectic and at a temperature ≅2–3 K above. The other metatectic point has a composition slightly above the eutectic and a temperature also not much higher than that invariant point, making its detection very difficult.
- There are five monophasic solid domains. Three of them are well established by the multiple techniques used, but the two domains associated to the metatectic point are very narrow and were not possible to individualize.
- Four biphasic solid–solid domains were observed along with five solid–liquid domains. The presence of all these two-phase domains was confirmed by the spectroscopic and microscopic techniques here used.

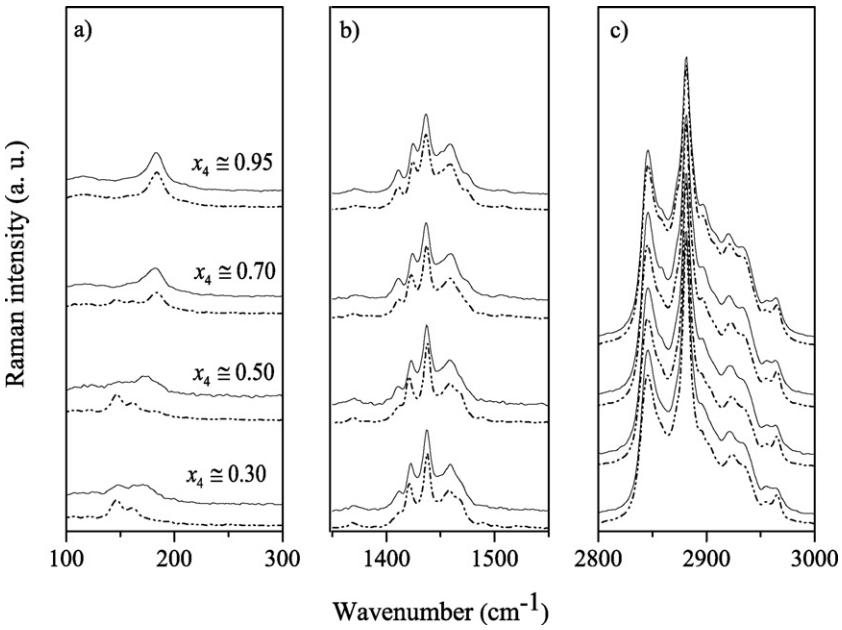

Fig. 5. FT-Raman spectra for myristic acid (4) + stearic acid (6) system at 313.15 K. The dashed lines represent the spectra before melting and the solid lines after melting. The compositions for (b) and (c) are the same presented in (a).

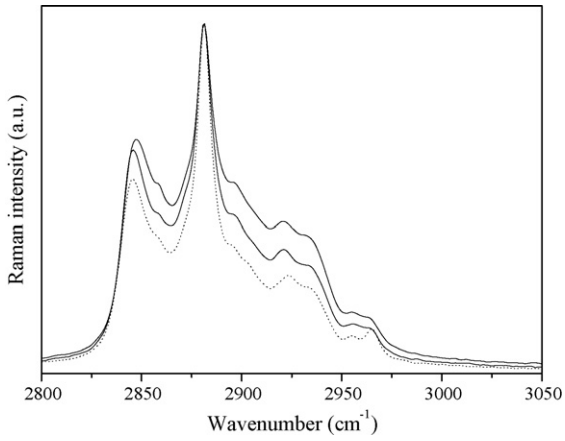

Fig. 6. FT-Raman spectra for myristic acid (4) + stearic acid (6) system at 322.15 K in the range 2800–3050 cm^{-1}. Dashed line represents the sample ($x_4 \cong 0.50$) before melting; from top to bottom: $x_4 \cong 0.55$, $x_4 \cong 0.50$.

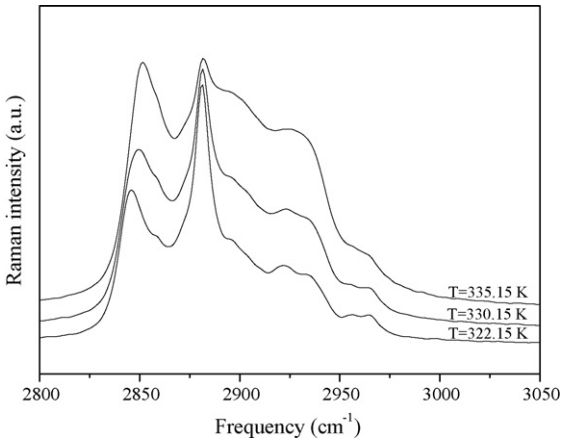

Fig. 7. FT-Raman spectra for myristic acid (4) + stearic acid (6) system at $x_4 \cong 0.30$ in the range 2800–3050 cm^{-1}.

If the thermograms of the binaries studied produced the first hints to the complexity of their phase diagrams, the plot of the enthalpies of the peaks associated to the eutectic and peritectic points as function of the composition of the mixture (Tamman plot) presented in Fig. 2, made possible the identification of the range of concentrations of the two phase regions associated with these points (Chernik, 1995; Inoue et al., 2004a,b). Tamman plots were drawn for the mixtures studied and the plot for the system of capric acid (2) + myristic acid (4) is presented in Fig. 3 as example. They show that neither of the biphasic regions extends to the pure compounds as would be expected from the classical interpretation of these diagrams (Abrams and Prausnitz, 1975), showing that a region of complete mutual solubility exists at extremes of the phase diagram. It is also possible to confirm with these plots that the eutectic point is located for all mixtures at a molar fraction of ≅0.8.

3.2. FT-Raman spectroscopy

The Raman bands of pure acids were assigned based on *ab initio* calculations for monomers and dimers, following the methodology described elsewhere (Nolasco et al., 2006; Costa et al., accepted for publication). The Raman spectra of pure acids were found to be mainly described by the calculated spectrum for the corresponding monomer. Notable exceptions are the bands related with the carboxylic group (which can be qualitatively described by the dimer spectra) and the bands arising from Fermi resonance. The final assignments are in general agreement with previous empirical assignments (Brown et al., 1987).

The FT-Raman spectra show different vibration modes for different crystal forms of fatty acids and its melting (Brown et al., 1987; Garti and Sato, 1989; Tandon et al., 2000). Although the changes with composition and temperature of the samples can be observed in the whole spectrum, the present discussion will be focused on the three main spectral regions: 100–300, 1350–1550, and 2800–3000 cm^{-1}, shown in Fig. 4 for the myristic acid (4) + stearic acid (6) system.

In the spectra of the crystal forms, the first region is dominated by the strong band assigned to the LAM-3 vibrational mode (longitudinal acoustic mode—CCC angle deformation). This moderately sharp band is no longer observed in the melt, thus providing a probe to monitor the solid–liquid phase transition.

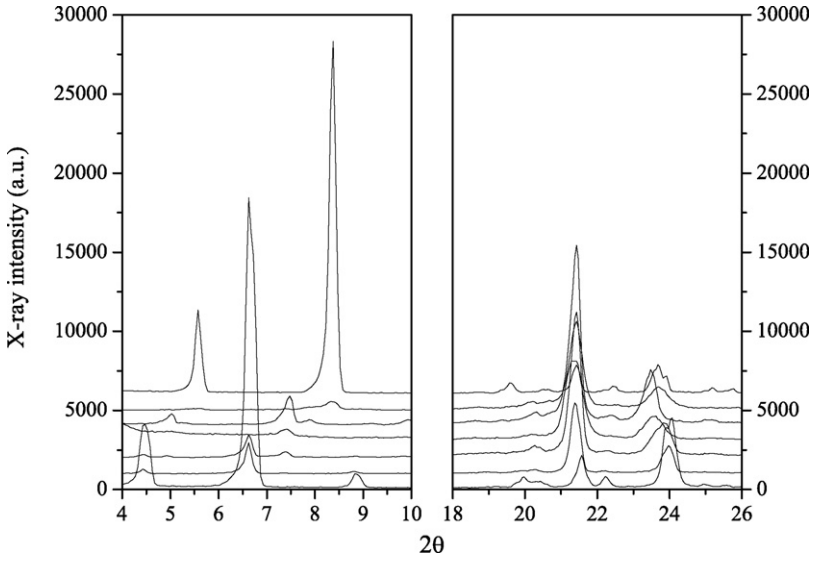

Fig. 8. X-ray powder diffraction patterns for the system myristic acid (4) + stearic acid (6). From top to bottom: $x_4 = 1.00$, $x_4 \cong 0.95$, $x_4 \cong 0.65$, $x_4 \cong 0.55$, $x_4 \cong 0.25$, $x_4 \cong 0.05$ and $x_4 = 0.00$; (a) range $4^\circ \leq 2\theta \leq 10^\circ$; (b) range $18^\circ \leq 2\theta \leq 26^\circ$.

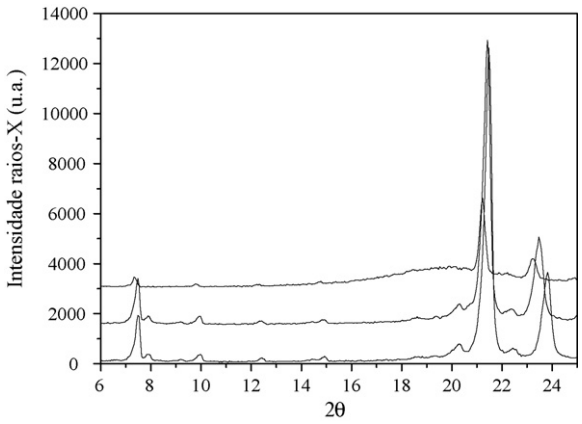

Fig. 9. X-ray powder diffraction patterns for the system myristic acid (4) + stearic acid (6) at constant composition $x_4 \cong 0.65$. From top to bottom: $T = 322.15$ K, $T = 318.15$ K and 303.15 K.

The 1350–1550 cm^{-1} region is ascribed to CH_2 and CH_3 bending modes. It has also been found to be sensitive to temperature variations and phase transition. In particular, both the higher wavenumber component at *ca.* 1460 cm^{-1} – assigned to the CH_3 bending mode – and the low wavenumber bands at *ca.* 1410 cm^{-1} and 1425 cm^{-1} – assigned to CH_2 bending modes – loose intensity upon temperature increase. In the liquid phase spectra these bands are only observed as shoulders of the central band.

In the third region, 2800–3050 cm^{-1}, only the bands ascribed to the CH stretching modes (νCH) are expected. However, these modes are strongly disturbed by several Fermi resonances (Lewis and McElhaney, 2002), leading to a complex band profile. The whole profile is sensitive to both temperature variation and phase transition. The intensity ratio of the two main peaks (at *ca.* 2845 and 2881 cm^{-1}, in the crystal phase), assigned to the symmetric and asymmetric CH_2 stretching modes, respectively, has been used to evaluate the *trans*/*gauche* conformational ratio within the chains (Lewis and McElhaney, 2002). In addition, the Fermi resonance components at higher wavenumber are strongly intensified in the liquid phase, providing a clear distinction between crystal phase and liquid phase band profiles.

To evaluate if the solid phase region of the phase diagrams was composed of the pure fatty acids plus an intermediate compound, as suggested by the classical interpretation of these phase diagrams, physical mixtures of the pure compounds were prepared and their Raman spectra collected before melting the sample and compared with the spectra collected after melting and recrystallization of the sample. Raman spectra for the myristic acid (4) + stearic acid (6) system at 313.15 K before sample melting (physical mixture, dashed

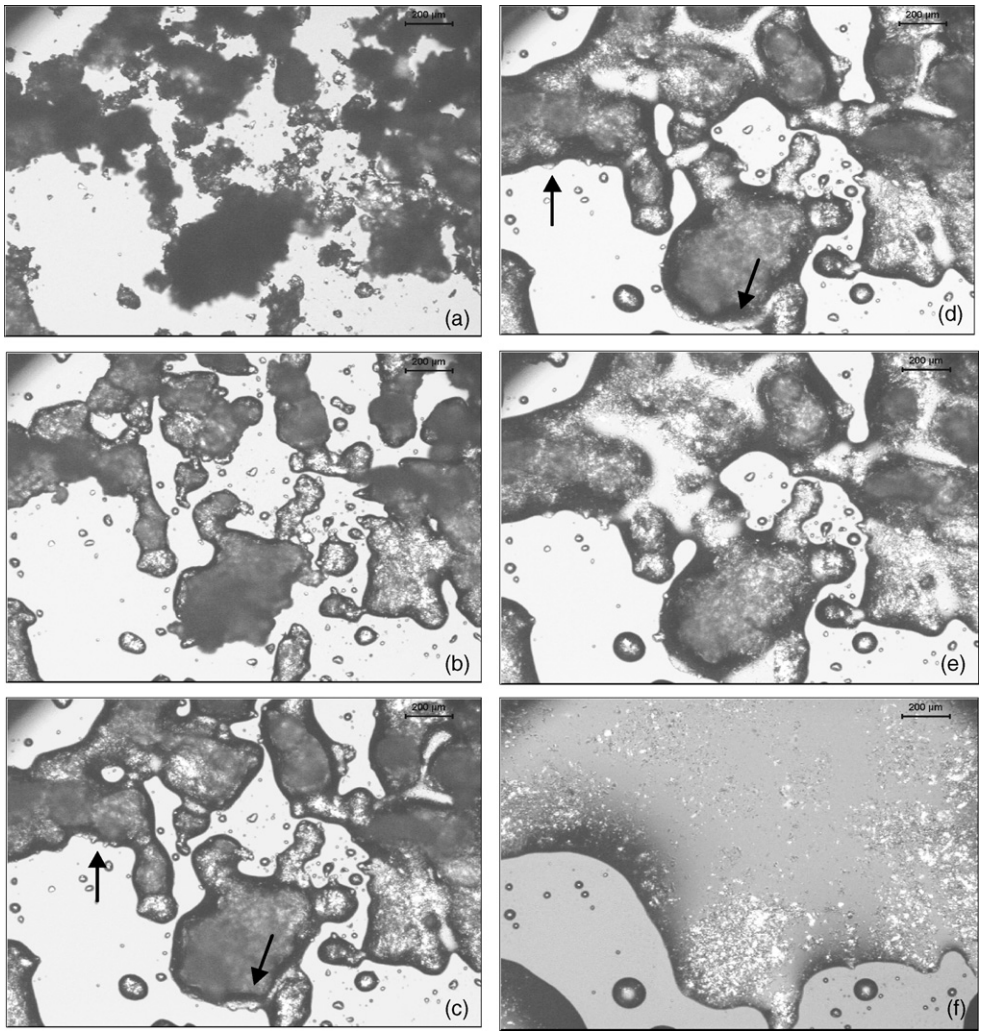

Fig. 10. Microscopy images of the system myristic acid (4) + stearic acid (6) + at $x_4 \cong 0.50$. (a) 323.15 K; (b) 325.15 K; (c) 326.15 K; (d) 326.65 K; (e) 327.15 K; and (f) 331.15 K.

line) and after sample melting (solid line), in the three spectral regions discussed above are presented in Fig. 5.

As can be seen in Fig. 5(a), the two LAM-3 bands belonging to myristic acid ($\cong$185 cm^{-1}) and to stearic acid ($\cong$147 cm^{-1}) are observed in the spectra of physical mixtures (BM), for all compositions (due to the low concentration only weak bands are observed for $x_4 = 0.30$ and $x_4 = 0.95$). However, after melting and cooling to the same temperature, only a single band with its maximum at an intermediate value of the pure acids is observed, clearly indicating that the after-melting mixture is not just a mixture of two pure solids.

The same general behavior is observed in the 1400–1500 cm^{-1} region (Fig. 5b). While the band at *ca.* 1410 cm^{-1} remains nearly unchanged, the band at *ca.* 1425 cm^{-1} is shifted upwards and looses intensity after sample melting and recrystallization.

The νC–H region (Fig. 5c), provides additional information concerning the nature of the samples after melting. In comparison with the physical mixture, the spectra of the samples after melting present a decrease of the (2881 cm^{-1})/(2845 cm^{-1}) intensity ratio and a moderate intensity increase in the higher wavenumber side of the band profile (*ca.* 2900–2950 cm^{-1}). These effects present a maximum for $x_4 \cong 0.50$. Both effects are associated with increase of conformational disorder. In particular, the decrease of the (2881 cm^{-1})/(2845 cm^{-1}) intensity ratio indicates an increase of the *gauche* conformations within the carbon chain probably associated with the defects at the lamellar interface of the C_i phase as discussed by Dorset (2004). The effect is even more dramatic at higher temperatures.

Fig. 6 presents the Raman spectra in the 2800–3050 cm^{-1} for sample composition $x_4 \cong 0.50$ and $x_4 \cong 0.55$, at 322.15 K. The comparison of the spectra shows little difference indicating that both are in the solid phase and no liquid was presence. The absence of liquid for a temperature and composition of the $x_4 \cong 0.50$ is not compatible with the classical interpretation of this phase diagram after which the mixture under these conditions should be partially in the liquid state. The absence of liquid at this temperature and concentration range is in good agreement with the global phase diagram sketched in Fig. 1.

The FT-Raman spectra for the system myristic acid (4) + stearic acid (6) at $x_4 \cong 0.30$ with the increase of the temperature is presented in Fig. 7. According to the classical interpretation, the region between 328 and 333 K for this system is a region of solid–liquid equilibrium. However, the spectra in Fig. 7 clearly show the absence of liquid in this region. This observation is not compatible with the classical phase diagram of type 2-Ib2 and the existence of liquid, observed in this figure at 335.15 K, confirm the existence of a SLE region, corroborate to the global phase diagram herein proposed.

3.3. X-ray diffraction

The diffraction patterns of the studied mixtures show some particularities that corroborate the global phase diagram sketched in Fig. 1. Fig. 8 shows the diffraction patterns at 313.15 K of the system myristic acid (4) + stearic acid (6) at different compositions in the range of $4^\circ \leq 2\theta \leq 10^\circ$ and $18^\circ \leq 2\theta \leq 26^\circ$. The first important observation is the similarities between the diffraction pattern of the pure fatty acids with the mixtures $x_4 \cong 0.95$ and $x_4 \cong 0.05$. Both mixtures presents almost same diffraction pattern, except for the disappearing of some very small peaks present in the pure fatty acid in which the mixture is richer and for the decrease of the intensity principally in the region of small angle. The fact that the diffraction pattern of these mixtures at 313.15 K, $x_4 \cong 0.05$ and $x_4 \cong 0.95$, are very similar with those of pure fatty acids and without evidence for the presence of the second fatty acid sustains, along with the Tamman plot results described above, the existence of a monophasic region of solid solution, *C*, on the extremes of phase diagram.

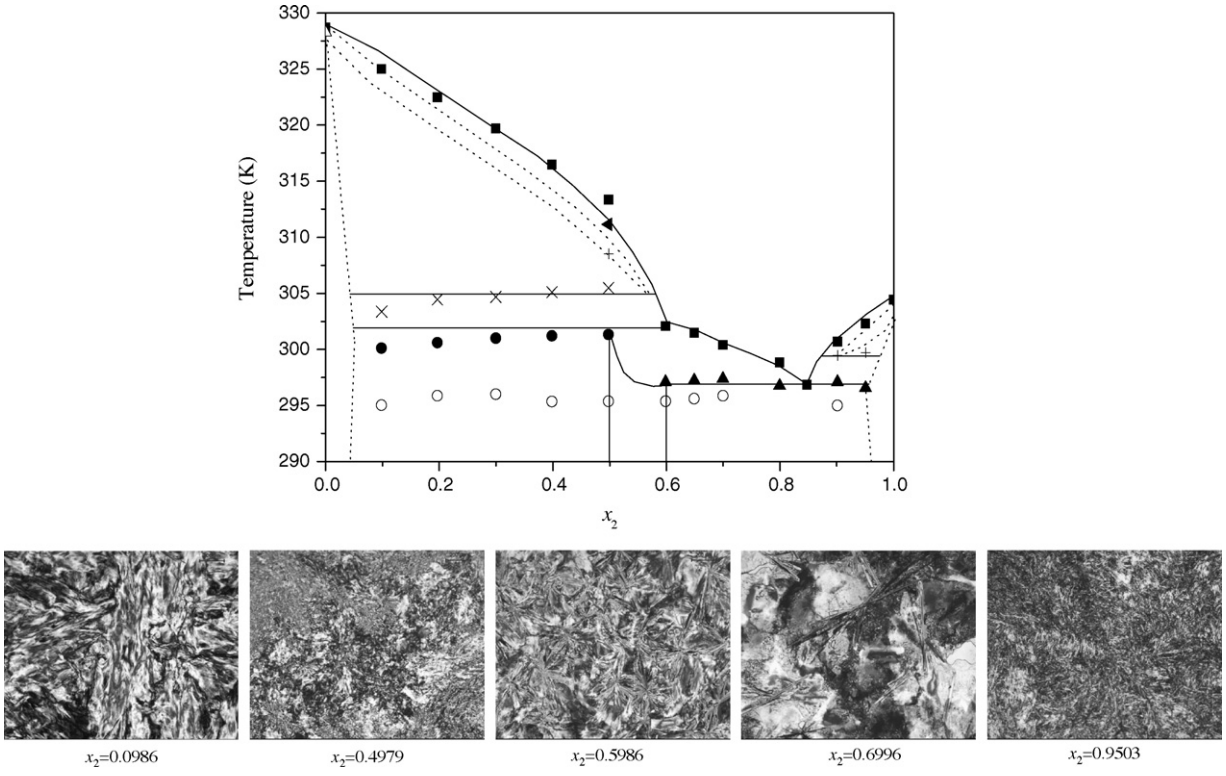

Fig. 11. Phase diagram of the system capric acid (2) + myristic acid (4) and images of this system. (■) Fusion temperature; (●) peritectic temperature; (▲) eutectic temperature; (×) metatectic temperature; (+, ○, ◄) transitions temperatures on the solid phase; (△) transition on the solid phase of the pure component.

Also in Fig. 8a, for $x_4 \cong 0.25$, it is possible to observe the appearance of a new peak at $2\theta \cong 7.5^\circ$. This peak is attributed to the new phase C_i and at this composition the C_i phase coexists with the C phase for which the peaks observed at $x_4 \cong 0.05$ are still present. With the increase of the myristic acid concentration in the mixture, for $x_4 \cong 0.55$, the peak related to the C_i phase at $2\theta \cong 7.5^\circ$, is the unique peak observed indicating the existence of a monophasic region, C_i, with complete miscibility of two fatty acids. With the increase of the myristic acid concentration in the mixture, at $x_4 \cong 0.65$ another peak, $2\theta \cong 8^\circ$, corresponding to the C phase observed in the myristic acid rich region, appears and coexists with the C_i phase until concentrations close to $x_4 \cong 0.95$ where, as discussed above, only a peak akin to that of the pure myristic acid, although less intense, is observed. In Fig. 8b, in the region $18^\circ \leq 2\theta \leq 26^\circ$, the appearance of a new peak is not observed unlike in our previous work (Costa et al., accepted for publication). Only a small shift to the left of the peak at approximately $2\theta \geq 23.9$ and a loss of intensity indicates the existence of new crystal structure for $x_3 \cong 0.55$. The diffraction patterns at 313.15 K clearly indicate the presence of the five regions sketched in the global phase diagram: three monophasic regions and two biphasic regions.

The effect of the temperature on the diffractograms was evaluated for the same compositions discussed above. Unfortunately most solid phases present very similar powder diffractograms, making it very hard to distinguish between them and to observe the solid–solid transitions present in the phase diagram. Yet in some cases it is possible to collect interesting information from them that support the proposed phase diagram.

At a composition of $x_4 \cong 0.65$, shown in Fig. 9, the changes on the diffraction pattern clearly follow the phase diagram proposed. The diffraction patterns show that with the increase of the temperature of 303.15–318.15 K a shift of the peak at $2\theta \cong 24^\circ$ is observed,

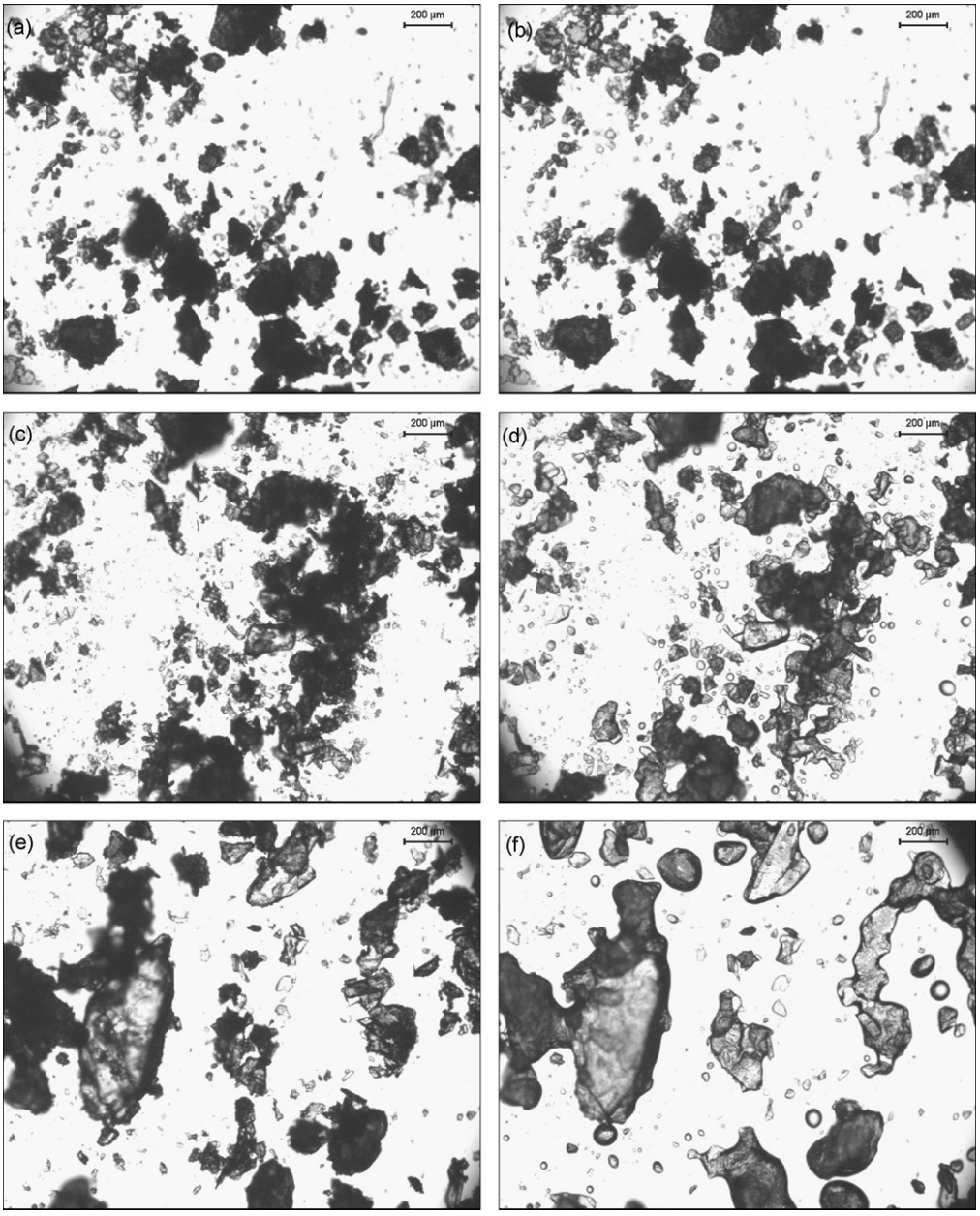

Fig. 12. Microscopy images of the system myristic acid (4) + stearic acid (6). (a and b) $x_4 \cong 0.50$; (c and d) $x_4 \cong 0.55$; (e and f) $x_4 \cong 0.60$; the left column at 318.15 K and right column at 322.15 K.

indicating a rearrangement of the crystal due the increase of the temperature. When the temperature further increases from 318.15 to 322.15 K it is possible to observe that only the peaks related to the phase C_i, $2\theta \cong 7^\circ$, remain while the melting of the other phase is confirmed by the broadening of the peaks and the baseline deviation of the diffraction pattern.

3.4. Polarized light microscopy

Isothermal sections at room temperature and temperature scans of samples for a number of mixtures were carried out with polarized light microscopy aiming at showing the presence of multiple regions in the phase diagram at low temperatures, and to confirm and elucidate one of the most peculiar features of these phase diagrams: the biphasic region ($C+l$) below the metatectic point.

Images for the myristic acid (4) + stearic acid (6) system with $x_4 = 0.50$, obtained in the temperature range between 323 and 333 K, while heating the sample at 0.1 K min^{-1}, are presented in Fig. 10. Fig. 10a, 323.15 K, shows the sample still completely solid, being possible to observe the crystals in thin overlapped layers and presenting an irregular shape. With the increase of the temperature to 325.15 K the shape of the crystals change becoming round due a partial melting of these crystals like as shown in Fig. 10b. In Fig. 10c, 326.65 K, the amount of liquid is larger than in the previous image but it is possible to see the liquid formed undergoing a recrystallization. No liquid is observed at 327.15 K in Fig. 10d and the small quantities of liquid previously formed are now in the solid state, as indicated by the black arrow in the figure. At 327.65 K, Fig. 10e, is possible observe that the sample is again melting with almost complete disappearing of the crystals marked by the black arrows in Fig. 10d. Finally at 331.15 K, Fig. 10f, the sample partly melted presents a regular shape on the borders, the few crystals existents are visible as white points on the figure. These results attest the presence of the two-phase region ($C+l$), and that during heating the sample undergoes a partial melting followed by a recrystallization of the sample.

The presence of multiple regions in the phase diagram at low temperatures was also observed using the polarized microscopy and results are reported for one of the systems, capric acid (2) + myristic acid (4), along with the phase diagram in Fig. 11. The images show the different crystals arrangements for each region presented on the global phase diagram, corroborating the presence of multiple phases at low temperature.

Accordingly to the conventional interpretation of these phase diagrams as a type 2-Ib2 phase diagram (Nývlt, 1977) it would be impossible the existence of liquid before the peritectic point, observed for the system myristic acid + stearic acid at approximately $x_4 \cong 0.62$. Fig. 12 shows images of the system myristic acid + stearic acid at 318.15 and 322.15 K for $x_4 \cong 0.50$, $x_4 \cong 0.55$ and $x_4 \cong 0.60$. For the lower temperature the sample is solid at all compositions as shown in Fig. 12a, c and e. With the increase of the temperature for 322.15 K no changes are observed in Fig. 12b, but for Fig. 12d is possible see a lot of crystals, now, with a round shape indicating the existence of liquid at this temperature. The same happens in Fig. 12f in larger quantities than for the previous composition according to the lever rule. The existence of liquid before the peritectic point, as shown in Fig. 12 at 322.15 K, also corroborates the global phase diagram proposed in Fig. 1.

3.5. Complete phase diagrams for the binary mixtures of consecutive, even saturated fatty acids

The global phase diagram proposed, and for which support was derived using the various techniques applied in this work, was now

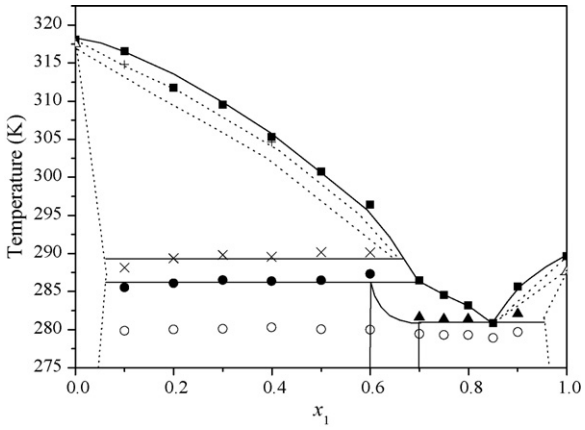

Fig. 13. Phase diagram of the system caprylic acid (1) + lauric acid (3). (■) Fusion temperature; (●) peritectic temperature; (▲) eutectic temperature; (×) metatectic temperature; (+, ○) transitions temperatures on the solid phase; (△) transition on the solid phase of the pure component.

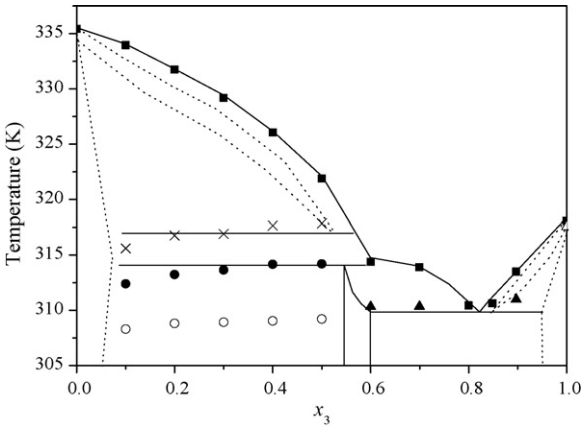

Fig. 14. Phase diagram of the system lauric acid (3) + palmitic acid (5). (■) Fusion temperature; (●) peritectic temperature; (▲) eutectic temperature; (×) metatectic temperature; (○) transition temperature on the solid phase; (△) transition on the solid phase of the pure component.

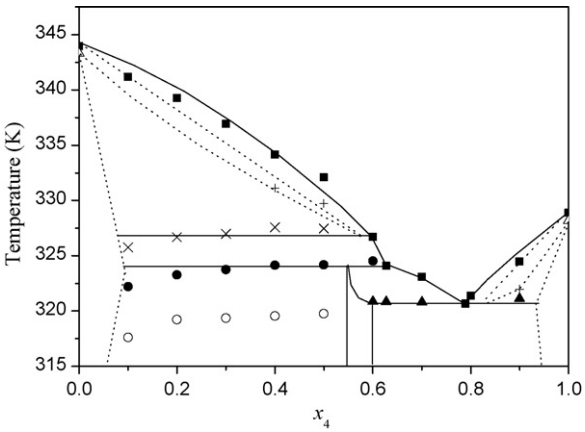

Fig. 15. Phase diagram of the system myristic acid (4) + stearic acid (6). (■) Fusion temperature; (●) peritectic temperature; (▲) eutectic temperature; (×) metatectic temperature; (+, ○) transitions temperatures on the solid phase; (△) transition on the solid phase of the pure component.

used to interpret the phase transition obtained from the thermograms and reported in Tables 1–4. The results are presented in Figs. 11 and 13–15.

The metatectic reaction of the right side of the phase diagram was observed just in one of the systems presented here, myristic acid (4) + stearic acid (6), Fig. 15. Due to the proximity of the metatectic and the eutectic temperatures the peaks of these transitions overlap making it difficult to individualize the metatectic transition. It is also difficult to separate the transitions associated to the C_h monophasic regions.

3.6. Conclusions

It was here presented for the first time the complete solid–liquid phase diagrams of binary mixtures of saturated fatty acids formed by caprylic acid ($C_{8:0}$) + lauric acid ($C_{12:0}$), capric acid ($C_{10:0}$) + myristic acid ($C_{14:0}$), lauric acid ($C_{12:0}$) + palmitic acid ($C_{16:0}$) and myristic acid ($C_{14:0}$) + stearic acid ($C_{18:0}$).

Using differential scanning calorimetry complemented with XRD, FT-Raman spectroscopy and polarized light microscopy measurements it was possible to show that the conventional interpretation of these phase diagrams was not correct and to identify the existence of, besides the peritectic and eutectic reactions, also the occurrence of a metatectic reaction and regions of complete miscibility between the fatty acids on the extremes of phase diagram and at intermediate values of concentration. It is shown that, unlike previously admitted, the phase diagrams for these systems are quite complex with important impacts on the design of separation and purification process for fatty acids and also on the development of products based on these compounds.

Acknowledgments

The authors are grateful to CNPq (nos. 141607/2004-1, 142823/2005-8 and 303649/2004-6), FAPESP (no. 2005/53095-2), CAPES-GRICES (0148/06-7), FAEPEX/UNICAMP FEDER and Fundação para a Ciência e a Tecnologia through project POCI/CTM/60288/2004 and PhD grant SFRH/BD/23400/2005 for financial support.

References

Abrams, D.S., Prausnitz, J.M., 1975. Statistical thermodynamics of liquid-mixtures—new expression for excess Gibbs energy of partly or completely miscible systems. AICHE J. 21 (1), 116–128.
Bailey, A.E., 1950. Melting and Solidification of Fats. Interscience Publishers, New York.
Brown, K.G., Bicknell-Brown, E., Ladjadj, M., 1987. Raman-active bands sensitive to motion and conformation at the chain termini and backbones of alkanes and lipids. J. Phys. Chem. 91, 3436–3442.
Carvalho, I.S., Miranda, I., Pereira, H., 2006. Evaluation of oil composition of some crops suitable for human nutrition. Ind. Crops Prod. 24 (1), 75–78.
Chapman, D., 1962. Polymorphism of glycerides. Chem. Rev. 62 (5), 433–456.
Chernik, G.G., 1995. Phase-equilibria in phospholipid water-systems. Adv. Colloid Interface Sci. 61, 65–129.
Costa, M.C., Krähenbühl, M.A., Meirelles, A.J.A., Daridon, J.L., Pauly, J., Coutinho, J.A.P., 2007a. High pressure solid–liquid equilibria of fatty acids. Fluid Phase Equilibr. 253 (2), 118–123.
Costa, M.C., Rolemberg, M.P., Boros, L.A.D., Krähenbühl, M.A., Oliveira, M.G., Meirelles, A.J.A., 2007b. Solid–liquid equilibrium of binary fatty acids mixtures. J. Chem. Eng. Data 52, 30–36.
Costa, M.C., Sardo, M., Rolemberg, M.P., Coutinho, J.A.P., Meirelles, A.J.A., Ribeiro-Claro, P., Krähenbühl, M.A., accepted for publication. The complete solid–liquid phase diagrams of binary mixtures of consecutive, even saturated fatty acids. Chem. Phys. Lipids.
Dorset, D.L., 2004. Crystallography of the Polymethylene Chain: An Inquiry into the Structure of Waxes. Oxford University Press.
Falk, O., Meyer-Pittroff, R., 2004. The effect of fatty acid composition on biodiesel oxidative stability. Eur. J. Lipid Sci. Technol. 106 (12), 837–843.
Garti, N., Sato, K., 1989. Crystallization and Polymorphism of Fats and Fatty Acids. Marcel Dekker, New York.
Goto, M., Asada, E., 1978a. Crystal-Structure of a-Super Form of Lauric Acid. Bull. Chem. Soc. Jpn. 51 (1), 70–74.
Goto, M., Asada, E., 1978b. Crystal-Structure of B-Form of Stearic-Acid. Bull. Chem. Soc. Jpn. 51 (9), 2456–2459.
Holland, R.F., Nielsen, J.R., 1963. A new crystal form of fatty acids. Acta Crystallogr. 16 (9), 902–906.
Inoue, T., Hisatsugu, Y., Ishikawa, R., Suzuki, M., 2004a. Solid–liquid phase behavior of binary fatty acid mixtures 2. Mixtures of oleic acid with lauric acid, myristic acid, and palmitic acid. Chem. Phys. Lipids 127 (2), 161–173.
Inoue, T., Hisatsugu, Y., Suzuki, M., Wang, Z., Zheng, L., 2004b. Solid–liquid phase behavior of binary mixtures 3. Mixtures of oleic acid with capric acid (decanoic acid) and caprylic acid (octanoic acid). Chem. Phys. Lipids 132, 225–234.
Inoue, T., Hisatsugu, Y., Yamamoto, R., Suzuki, M., 2004c. Solid–liquid phase behavior of binary fatty acid mixtures 1. Oleic acid stearic acid and oleic acid behenic acid mixtures. Chem. Phys. Lipids 127 (2), 143–152.
Iwahashi, M., Takebayashi, S., Taguchi, M., Kasahara, Y., Minami, H., Matsuzawa, H., 2005. Dynamical dimer structure and liquid structure of fatty acids in their binary liquid mixture: decanoic/octadecanoic acid and decanoic/dodecanoic acid systems. Chem. Phys. Lipids 133 (2), 113–124.
Johnson, R.W., Fritz, E., 1989. Fatty Acids in Industry: Processes, Properties, Derivatives, Applications. Marcel Dekker, Nova York.
Kaneko, F., Kobayashi, M., Kitagawa, Y., Matsuura, Y., 1990. Structure of Stearic-Acid E-Form. Acta Crystallogr. C 46, 1490–1492.
Karleskind, A., 1996. Oils & Fats Manual: A Comprehensive Treatise, Properties, Production, Applications. Lavoisier Publishing, Paris.
Kogan, A., Garti, N., 2006. Microemulsions as transdermal drug delivery vehicles. Adv. Colloid Interface Sci. 123, 369–385.
Lewis, R., McElhaney, R., 2002. Vibrational spectroscopy of lipids. In: Chalmers, J.M., Griffiths, P.R. (Eds.), Handbook of Vibrational Spectroscopy, vol. 5. Wiley, pp. 3447–3464.
Lomer, T.R., 1963. Crystal and molecular structure of lauric acid (Form a1). Acta Crystallogr. 16 (10), 984–988.
Meher, L.C., Sagar, D.V., Naik, S.N., 2006. Technical aspects of biodiesel production by transesterification—a review. Renew. Sustain. Energy Rev. 10 (3), 248–268.
Moreno, E., Cordobilla, R., Calvet, T., Cuevas-Diarte, M.A., Gbabode, G., Negrier, P., Mondieig, D., Oonk, H.A.J., 2007. Polymorphism of even saturated carboxylic acids from *n*-decanoic to *n*-eicosanoic acid. New J. Chem. 31, 947–957.
Nolasco, M.M., Amado, A.M., Ribeiro-Claro, P.J.A., 2006. Computationally-assisted approach to the vibrational spectra of molecular crystals: study of hydrogen-bonding and pseudo-polymorphism. Chemphyschem 7 (10), 2150–2161.
Nývlt, J., 1977. Solid–liquid Phase Equilibria. Elsevier, Amsterdam.
Sato, K., 2001. Crystallization behaviour of fats and lipids—a review. Chem. Eng. Sci. 56, 2255–2265.
Sato, K., Ueno, S., Yano, J., 1999. Molecular interactions and kinetic properties of fats. Prog. Lipid Res. 38 (1), 91–116.
Shilei, L., Neng, Z., Guohui, F., 2006. Eutectic mixtures of capric acid and lauric acid applied in building wallboards for heat energy storage. Energy Buildings 38, 708–711.
Small, D.M., 1986. Physical Chemistry of Lipids: From Alkanes to Phospholipids. Plenum press, New York and London.
Tandon, P., Forster, G., Neubert, R., Wartewig, S., 2000. Phase transitions in oleic acid as studied by X-ray diffraction and FT-Raman spectroscopy. J. Mol. Struct. 524, 201–215.
Timms, R.E., 1984. Phase behaviour of fats and their mixtures. Prog. Lipid Res. 23, 1–38.
Vand, V., Morley, W.M., Lomer, T.R., 1951. The crystal structure of lauric acid. Acta Crystallogr. 4 (4), 324–329.
Zhang, J.J., Zhang, J.L., He, S.M., Wu, K.Z., Liu, X.D., 2001. Thermal studies on the solid–liquid phase transition in binary systems of fatty acids. Thermochim. Acta 369 (1–2), 157–160.